International Journal of Remote Sensing, 2015
Vol. 36, No. 22, 5537–5556, http://dx.doi.org/10.1080/01431161.2015.1101505

Taylor & Francis
Taylor & Francis Group

A novel approach for the characterization of tundra wetland regions with C-band SAR satellite data

Barbara Widhalm[a,b]*, Annett Bartsch[a,b,c], and Birgit Heim[d]

[a]*Department of Geodesy and Geoinformation, Research group Remote Sensing, Vienna University of Technology, Vienna 1040, Austria;* [b]*Austrian Polar Research Institute, c/o Universität Wien, 1090 Vienna, Austria;* [c]*Section Climate Change Impacts, ZAMG- Zentralanstalt für Meteorologie und Geodynamik, Vienna 1190, Austria;* [d]*Hemholtz-Zentrum für Polar und Meeresforschung, Periglacial Research, Alfred Wegener Institute, Potsdam 14473, Germany*

(*Received 27 April 2015; accepted 11 September 2015*)

A circumpolar representative and consistent wetland map is required for a range of applications ranging from upscaling of carbon fluxes and pools to climate modelling and wildlife habitat assessment. Currently available data sets lack sufficient accuracy and/or thematic detail in many regions of the Arctic. Synthetic aperture radar (SAR) data from satellites have already been shown to be suitable for wetland mapping. Envisat Advanced SAR (ASAR) provides global medium-resolution data which are examined with particular focus on spatial wetness patterns in this study. It was found that winter minimum backscatter values as well as their differences to summer minimum values reflect vegetation physiognomy units of certain wetness regimes. Low winter backscatter values are mostly found in areas vegetated by plant communities typically for wet regions in the tundra biome, due to low roughness and low volume scattering caused by the predominant vegetation. Summer to winter difference backscatter values, which in contrast to the winter values depend almost solely on soil moisture content, show expected higher values for wet regions. While the approach using difference values would seem more reasonable in order to delineate wetness patterns considering its direct link to soil moisture, it was found that a classification of winter minimum backscatter values is more applicable in tundra regions due to its better separability into wetness classes. Previous approaches for wetland detection have investigated the impact of liquid water in the soil on backscatter conditions. In this study the absence of liquid water is utilized.

Owing to a lack of comparable regional to circumpolar data with respect to thematic detail, a potential wetland map cannot directly be validated; however, one might claim the validity of such a product by comparison with vegetation maps, which hold some information on the wetness status of certain classes. It was shown that the Envisat ASAR-derived classes are related to wetland classes of conventional vegetation maps, indicating its applicability; 30% of the land area north of the treeline was identified as wetland while conventional maps recorded 1–7%.

Introduction

The representation of spatial wetness patterns is in great demand for research in Arctic environments, for example in upscaling of flux measurements, soil thermal properties

*Corresponding author. Email: barbara.widhalm@geo.tuwien.ac.at
Present affiliation for Barbara Widhalm is Section Climate Change Impacts, ZAMG- Zentralanstalt für Meteorologie und Geodynamik, Vienna 1190, Austria.

assessment (heat transfer), and general soil properties (aerobic/anaerobic conditions – carbon storage). Regional to global wetland products focus mostly on inundation fraction and its variation utilizing coarse-resolution (25–50 km) data sets (Prigent et al. 2007; Schroeder et al. 2010; Jones et al. 2011). Such data provide valuable information on seasonally waterlogged conditions and thus can be applied as a basis to estimate methane release (Durden et al. 1996; Morrissey et al. 1996; Ringeval et al. 2010; Watts et al. 2014). Soils close to saturation (especially in peatlands) however need to be considered as well for carbon land surface–atmosphere exchange studies (Schneider, Grosse, and Wagner 2009, Koven et al. 2011; van Huissteden and Dolman 2012). Microwave satellite data have been shown suitable for near-surface soil saturation retrieval (e.g. Wagner, Lemoine, and Rott 1999; Pathe et al. 2009; Reschke et al. 2012).

Although global data sets of surface soil moisture based on satellite data do exist, their spatial resolution is relatively coarse, similar to the inundation data sets (25–50 km) (e.g. Kerr et al. 2001; Njoku 2004; Naeimi, Bartalis, and Wagner 2009a, 2009b). With heterogeneity being a major challenge in the Arctic, higher-resolution products are essential (Högström et al. 2014). It has been shown that such wetland products (<150 m) are possible when using synthetic aperture radar (SAR) data (e.g. Bartsch et al. 2008), but data availability is still insufficient for spatially continuous circumpolar records to date (Reschke et al. 2012; Bartsch et al. 2012). However, a comprehensive record is available from medium-resolution SAR (specifically Envisat Advanced SAR Global Monitoring mode (GM, 1 km)), which can be utilized to derive general wetness patterns for the Arctic (Bartsch et al. 2009).

Wetland classes are also included in land-cover maps. However, the accuracy of land-cover products for Arctic regions, specifically classes related to wetland types, and the product utility for various applications remain largely uncertain (Krankina et al. 2011). Pflugmacher et al. (2011) compared coarse-resolution land cover maps like GlobCover, GLC-2000, and MODIS C4 and C5 for northern Eurasia and confirmed their low mean agreement in the northern taiga-tundra zone.

Wetland classes typical of tundra environments are also only partially included in the widely used Global Lakes and Wetland database (Lehner and Döll 2004; e.g. Bartsch et al. 2008).

The purpose of this study is to explore circumpolar Envisat ASAR GM backscatter behaviour in subarctic and Arctic environments with special emphasis on spatial wetness patterns. Flux studies often distinguish between three classes: dry, mixed, and wet (Parmentier et al. 2011). Such categories can, for example, be associated with certain classes of detailed land-cover maps developed for methane flux upscaling (Schneider, Grosse, and Wagner 2009).

Conventional land-cover maps are explored with respect to their C-band backscatter characteristics and wetness classes. A novel type of circumpolar wetland map based on surface scattering characteristics rather than land-cover classes is eventually proposed in order to meet the needs, in particular, of land-surface exchange upscaling studies. Such an approach may be also applicable to the data from the follow-on sensor Sentinel-1 on a regional basis but at higher spatial resolution.

1. Data sets

1.1. ASAR GM

The Advanced Synthetic Aperture Radar (ASAR) instrument on board ESA's Envisat satellite operated in C-band (5.3 GHz) in five different modes with varying temporal and spatial resolution from 30 m to 1 km, from 2002 to spring 2012. Among these,

the GM formed the background mission and was active whenever no other mode had been requested. Using the ScanSAR technique, GM provided low-esolution images (1 km) with a wide swath width of 405 km and incidence angles from 15° to 45° (ESA 2004). These data became accessible from 2005. Data availability in the Arctic is high (Bartsch et al. 2009) due to overlapping swaths related to the polar orbit and the low demand for higher-resolution acquisitions in these regions. All ASAR GM level 1b data used were acquired with HH-Polarization.

1.2. Circumpolar and regional land cover maps

1.2.1. Circumpolar Arctic Vegetation Map

The Circumpolar Arctic Vegetation Map (CAVM, Walker et al. 2002) shows the types of vegetation that occur across the Arctic, between the ice-covered Arctic Ocean to the north and the northern limit of forests to the south. Its classes resemble vegetation communities and can be associated with the wetness levels dry, medium, and wet. It provides the source for the parameterization of the SAR-based classification approach.

A false-colour infrared image derived from biweekly 1993 and 1995 Advanced Very High Resolution Radiometer (AVHHR) data provided a base image for the interpretation of vegetation when the CAVM was developed. The approach used for making the CAVM was based on manual 'photo-interpretation' of the AVHRR satellite image mosaic. Vegetation is interpreted on the basis of 'integrated vegetation complexes' (IVC). These IVCs are derived from a combination of information from satellite-derived images and from existing source maps, such as bedrock geology, surficial geology, soils, hydrology, and previous vegetation maps. The CAVM is essentially a GIS database that uses expert knowledge of the relationship of plant communities to climate, parent material, and topographic factors to predict vegetation within landscape units that can be delineated on 1:7500-scale AVHRR images. (Walker et al. 2002).

Furthermore, the CAVM Team (2003) identified three different moisture levels for certain vegetation physiognomic units (see Table 1).

1.2.2. Global Boreal Forest Mapping Project

A data set was produced for Alaska and Siberia within the framework of the Global Boreal Forest Mapping Project (GBFM), an initiative of the Japan Aerospace Exploration Agency (JAXA), and is based on L-band Japanese Earth Resources Satellite 1 (JERS-1) data acquired in years 1997–1998.

The GBFM Siberia data set classification covers a major part of Siberia, with special attention to wetlands, and has a resolution of 100 m. Improved classification accuracy was obtained by taking terrain features into consideration (Kropacek and De Grandi 2006).

The thematic map of wetlands throughout Alaska (100 m resolution) was also produced using the GBFM data set. The classification was developed using the random forests decision tree algorithm with training and testing data compiled from the National Wetlands Inventory (NWI) and the Alaska Geospatial Data Clearinghouse (AGDC). The GBFM mosaics of summer and winter JERS-1 SAR imagery were employed together with other inputs and ancillary data sets (Whitcomb et al. 2009).

Table 1. CAVM classes (Walker et al. 2002) and wetness level categories.

Wetness level	CAVM class
Wet	12: Sedge/grass, moss wetland
	13: Sedge, moss, dwarf-shrub wetland
	14: Sedge, moss, low-shrub wetland
Medium	2: Rush/grass, forb, cryptogram tundra
	5: Graminoid, prostrate dwarf-shrub, forb tundra
	7: Non-tussock sedge, dwarf-shrub, moss tundra
	8: Tussock-sedge, dwarf-shrub, moss tundra
	9: Erect dwarf-shrub tundra
	10: Low-shrub tundra
Dry	1: Cryptogram, herb barren
	4: Prostrate dwarf-shrub, herb tundra
	6: Prostrate/hemiprostrate dwarf shrub tundra

1.2.3. United States Geological Survey Alaska

The United States Geological Survey (USGS) vegetation map of Alaska includes 19 vegetation classes (http://agdc.usgs.gov/data/usgs/erosafo/veg/vegetation.html) and has a resolution of 1 km. It uses the phenology of a vegetation index collected by the AVHRR during the 1991 growing season.

1.2.4. Northern Land Cover of Canada-Circa 2000

The Northern Land Cover of Canada-Circa 2000 (NLCC, Olthof, Latifovic, and Pouliot 2009) covers northern Canada north of the treeline and is based on medium-resolution (30 m) Landsat images which have been combined into 16 radiometrically balanced large-area mosaics. Spectral clusters were merged into 15 classes using look-up tables which were generated using existing land-cover products and limited field and additional reference data found in the literature.

1.2.5. Lena Delta

The Lena River Delta, situated in northern Siberia, is the largest Arctic delta and covers approximately 29,000 km^2. Remote sensing-derived regional land cover maps of the Lena Delta are publicly available from Schneider, Grosse, and Wagner (2009) and Muster et al. (2012a). Both Lena Delta data sets are derived from the same Landsat 7 ETM+ satellite data mosaic composed from cloud-free acquisitions in summer months in 2000 and 2001 at 30 m resolution. Schneider, Grosse, and Wagner (2009) applied supervised classification according training units taken from field descriptions and defined nine classes characterized by their vegetation, surface moisture, and topography. The map of wetness-related biome units was developed for upscaling of methane emissions. Muster et al. (2012b) used high-spatial resolution aerial photography to develop a statistical downscaling approach to derive the surface water fraction from the Landsat reflectances. Both data sets show the spatial distribution of three main wetness regimes related to the geomorphological main terraces of the Lena Delta: wet polygonal tundra on the first terrace, dry sparsely vegetated regime of the sandy second terrace, and the medium wetness regime of the third Yedoma terrace.

1.3. Global maps

1.3.1. Global Lakes and Wetlands Database

The Global Lakes and Wetlands Database (GLWD) is based on a variety of existing maps, data, and information. Its wetlands layer contains lakes, reservoirs, rivers, and different wetland types within a global raster map at 30″ resolution (Lehner and Döll 2004).

1.3.2. Climate Change Initiative

ESA's Climate Change Initiative (CCI) land-cover map is a global map at 300 m spatial resolution. It uses a multi-year, multi-sensor strategy and a legend based on the UN Land Cover Classification System (LCCS) (ESA 2009).

2. Methodology

Radar backscatter is dependent on sensor parameters such as incidence angle, polarization, and wavelength, geometric parameters like surface roughness and vegetation structure, as well as soil properties (Ulaby, Moore, and Fung 1982). Depicting material characteristics, the dielectric constant is highly dependent on soil moisture content, leading to higher backscatter values under wet soil conditions. In regions where mostly soil moisture contributes to the signal differences over time, wet areas can be determined by directly using backscatter values under unfrozen conditions (high–low corresponding to wet–dry, e.g. Wagner, Lemoine, and Rott (1999), Alvarez-Mozos et al. (2005), and Ulaby, Moore, and Fung (1982)). This requires homogenous scattering within the resolution cell, which is often not the case in Arctic wetland environments (Bartsch et al. 2010; Reschke et al. 2012; etc.). Especially for shorter wavelengths the penetration to the ground is limited in forests, hampering the detection of forested wetland patches. It also needs to be considered that there is a soil moisture threshold above which the saturated soil causes specular reflection leading to a decrease in radar backscatter (Henderson and Lewis 1998).

Temporal backscatter variations can be linked to soil moisture dynamics. Therefore time series-based approaches determine the location-specific dry (minimum) and wet (maximum) backscatter from time series records for unfrozen and non-snow-covered time periods to obtain the so-called dry and wet reference values (Wagner, Lemoine, and Rott 1999). By subtracting these reference images representing dry soil conditions from each radar image, surface roughness and land-cover patterns can be accounted for by change detection methods (Moran et al. 2000; Engman 2000).

However, in wetland areas which never dry out, this dry-reference value needs to be defined differently. In areas where freezing occurs, the frozen state backscatter can be used instead since the dielectric properties of frozen soil are similar to those of dry soil (Duguay et al. 2005; Naeimi et al. 2012). In both cases no or little liquid water is present. It has been postulated by Bartsch et al. (2012) that a combined use of dry-reference determination approaches (historical summer minimum and frozen records) can be used to identify wetlands in subarctic and Arctic environments. A significant difference between the dry references is expected for permanent wetlands. This method is hereafter referred to as 'difference' or 'diff'.

Snow cover and especially changes in snow structure can cause backscatter increase during winter in C-band (Naeimi et al. 2012). The backscatter minimum from Envisat ASAR GM under frozen conditions is therefore investigated for the month of December, which corresponds to the frozen period, and the impact of snow cover is considered to remain limited.

Arctic tundra regions are characterized by abundant lakes below the limits of GM resolution. This reduces the backscatter in summer and late winter when lakes freeze to the ground (Duguay and Lafleur 2003). It can be therefore assumed that the difference between summer and December is partially reduced in the case of a significant water fraction within the resolution cell. An alternative approach which utilizes only the December records is therefore now investigated.

For the required preprocessing of the Envisat ASAR GM level 1b data, the SAR Geophysical Retrieval Toolbox (SGRT, Vienna University of Technology, Sabel et al. 2012) was used. This is a collection of routines which manages SAR geocoding and radiometric calibration by calling other non-commercial and commercial software packages. By incorporating orbit information (DORIS (Doppler Orbitography and Radiopositioning Integrated by Satellite) orbit files) and digital elevation data (Shuttle Radar Topography Mission-improved U.S. Geological Survey GTOPO30 digital elevation model), othorectified images were produced at sub-pixel accuracy (Park et al. 2011; Pathe et al. 2009), depicting the backscatter coefficient σ_0 in dB. Resampling the data into a fixed 15 arc-seconds grid (datum WGS-84), within 0.5° by 0.5° tiles, further allowed efficient spatial and temporal analysis, designed for global processing. To remove the influence of local incidence angle on radar backscatter, the data (>8000 scenes north of 60° N) were normalized to a reference angle of 30° by fitting a linear model to the backscatter data (Pathe et al. 2009; Sabel et al. 2012, 2007).

Dry-reference maps were calculated from Envisat ASAR GM data for summer (July and August, hereafter referred to as $\sigma_{0,\ smin}$) and winter (December, hereafter referred to as $\sigma_{0,\ wmin}$) of the years 2005–2011, representing the minimum backscatter values of this timespan. $\sigma_{0,\ smin}$ can be seen as conditions of minimum soil moisture and therefore driest summer conditions, while $\sigma_{0,\ wmin}$ represents frozen conditions, which appear similar to dry conditions. December data are expected to show limited liquid water content and low impact by snow cover.

It is expected that regions with higher soil moisture exhibit higher backscatter and a greater decline in backscatter values in winter caused by freezing related to the drop in the dielectric constant. Therefore it is assumed that the difference between summer and winter dry reference is higher for wet regions than for dry ones.

Mean and median values, as well as standard deviation for vegetation classes of the circumpolar CAVM, were calculated for $\sigma_{0,\ wmin}$, $\sigma_{0,\ smin}$, and the difference between $\sigma_{0,\ wmin}$ and $\sigma_{0,\ smin}$ ($\sigma_{0,\ diff} = \sigma_{0,\ wmin} - \sigma_{0,\ smin}$) (see Figure 1). At this stage no masking of areas with high water fraction was applied for the circumpolar assessment.

The CAVM is the only circumpolar product with adequate thematic detail. Its moisture information, which can be assigned to several classes, was used in order to investigate the ASAR GM-derived backscatter in relation to wetness classes. In addition, the more detailed wetland map of Schneider, Grosse, and Wagner (2009) was used to evaluate and refine the backscatter stratification over the Lena Delta.

In the derived wetness level product, a mask for open water and glaciers was applied based on the map classes of GLWD (Lehner and Döll 2004) and GlobCover, (Bicheron et al. 2008), which is an ESA land-cover map based on Medium Resolution Imaging Spectrometer (MERIS), 300 m) sensor observations. All these data sets do not, however,

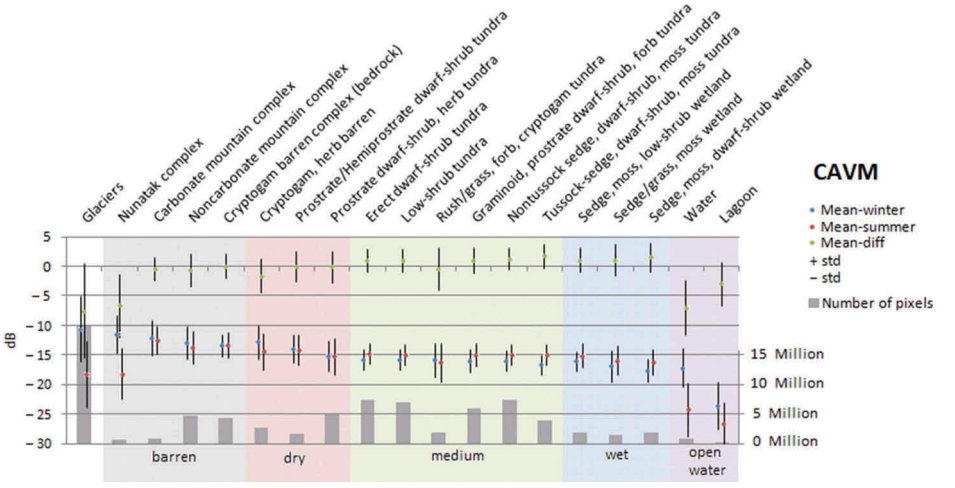

Figure 1. Mean values and standard deviations of $\sigma_{0,\,wmin}$, $\sigma_{0,\,smin}$, and $\sigma_{0,\,diff}$. ($= \sigma_{0,\,wmin} - \sigma_{0,\,smin}$) for CAVM classes ordered by wetness (grey: barren, mountainous; red: dry; green: medium; blue: wet; violet: open water).

completely capture open water bodies in the Arctic (Bartsch et al. 2008; Muster et al. 2013). An adequate circumpolar land-cover map is, to date, not available. The impact is discussed below.

Regions with backscatter ranges which can be associated with the wetness classes (as seen in Table 1) are compared to the conventional land-cover data sets listed in section 2.2.

Due to a lack of comparable data sets, the derived wetness level map was compared to land-cover maps containing classes of wetlands.

3. Results

3.1. Backscatter analysis

The analysis of backscatter statistics for CAVM classes showed that for both $\sigma_{0,\,wmin}$ and $\sigma_{0,\,smin}$, barren and sparsely vegetated areas exhibit highest backscatter values, followed by plant communities considered as dry (Figure 1). Vegetation community classes which can be found in moist areas showed lower backscatter values, with even lower values being encountered in wet areas and minimum values for open water bodies. The effect of roughness and volume scattering may thus be lower for wetter areas than for dry. Sub-pixel-size water bodies play an essential role in this environment and contribute to a reduction in backscatter in summer and increase in early winter.

In the $\sigma_{0,\,diff}$ product, negative values were found for barren areas and open water bodies; values increased from dry to wetter areas. Figure 1 shows that the wetter classes of the vegetation complexes of the CAVM (Table 1) show higher summer–winter differences than drier classes. This supports the hypothesis of Bartsch et al. (2012) that wetlands in this biome do not dry out in summer and can be therefore distinguished from other land cover when the expected backscatter value for dry conditions is known.

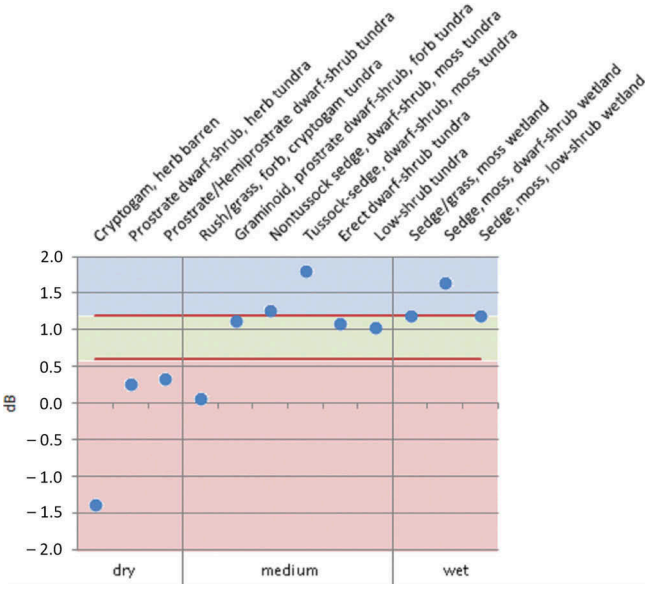

Figure 2. Median $\sigma_{0,\ \mathrm{diff}}$ values for dry, medium, and wet CAVM classes. Red lines indicate the chosen thresholds of 0.6 and 1.2 dB (red: dry; green: medium; blue: wet).

As apparent from Figure 2, $\sigma_{0,\ \mathrm{diff}}$ values for the wet and medium CAVM classes overlap, preventing a feasible separation of these classes within a potential wetness level product.

Only $\sigma_{0,\ \mathrm{wmin}}$ is therefore further used for extraction of wetness level maps (Figure 3). The mean between CAVM median backscatter values for each wetness level was used to set the thresholds to −15.2 and −16.5 dB. The median was used here instead of the mean due to its robustness concerning outliers. Figure 4 shows the resulting classes based on $\sigma_{0,\ \mathrm{wmin}}$.

A comparison with the medium-resolution (30 m) land cover map of the Lena Delta (Schneider, Grosse, and Wagner 2009) (Figure 5), as well as the global CCI Landcover product, was carried out as a first assessment step. It showed that the wetness level map reveals more detail than the global map but does not support the identification of the northern terrace which is characterized as 'dry moss-, sedge-, and dwarf shrub-dominated tundra' and comparably dry. With distinction of three wetness levels it is classified as wet. The comparison with $\sigma_{0,\ \mathrm{wmin}}$ (Figure 6) reveals that this area is characterized by even lower values. An additional class (class 'other') was therefore introduced in order to distinguish such open areas (sandbanks and flat sandy soils) as characteristic of a range of locations along Arctic coasts. The threshold for this class was set to −19 dB in $\sigma_{0,\ \mathrm{wmin}}$ to match the conditions in the field.

In the following the stratified map and its classes are referred to as wetness level map (WL map) and wetness level classes (WL classes), respectively.

3.2. *Comparison with conventional land cover*

To evaluate the WL map, the fraction of WL classes within each class of the used land-cover maps was assessed. For this purpose the land-cover maps were kept at their original resolution.

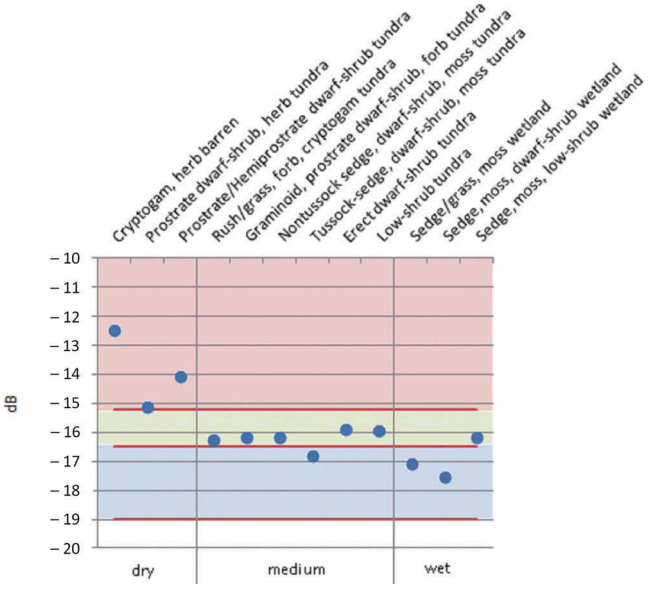

Figure 3. Median $\sigma_{0,\ \mathrm{wmin}}$ values for dry, medium and wet CAVM classes. Red lines indicate the chosen thresholds of −15.2, −16.5, and −19 dB (red: dry; green: medium; blue: wet).

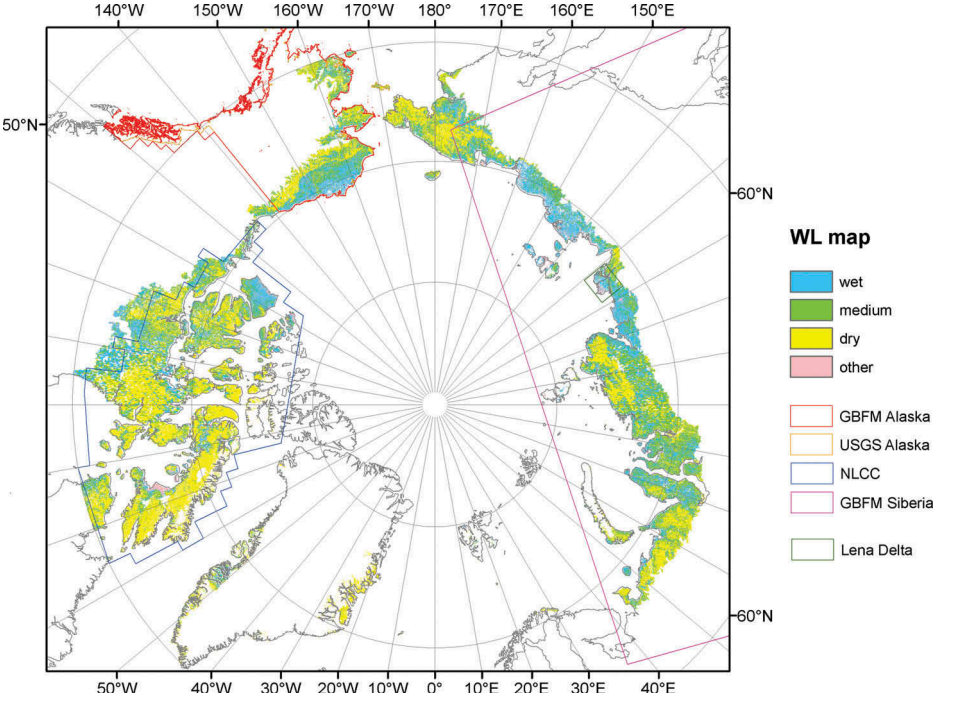

Figure 4. Wetness level map and outlines of the vegetation maps used for evaluation.

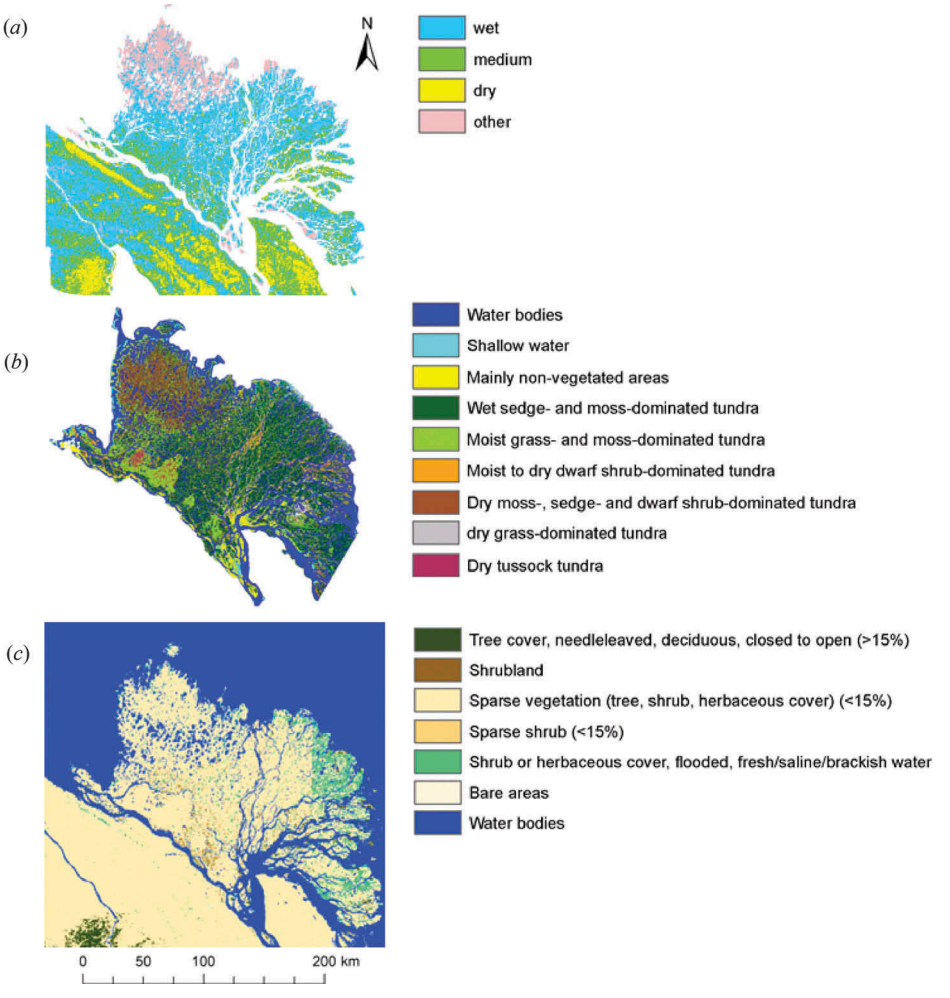

Figure 5. Comparison of the wetness level map (*a*) with the land-cover map of the Lena Delta (*b*, Schneider, Grosse, and Wagner 2009) and the CCI land cover map (*c*, ESA 2009).

3.2.1. *GBFM Siberia*

Comparison with the map GBFM Siberia showed that classes where the fraction of wet WL class pixels dominated are in fact to be considered as wet ('bogs', 'shallow water', 'water', Figure 7). Although the investigated area is situated north of the treeline as defined in the CAVM, a major portion of the GBFM Siberia map is classified as forest within this region. The class 'low biomass forest' shows similar fractions of wet, medium, and dry WL pixels and can be assumed to be medium class.

Even though the percentage of wet GBFM classes is considerably high within the dry WL class, the fraction increases for the medium and wet WL classes (Figure 8).

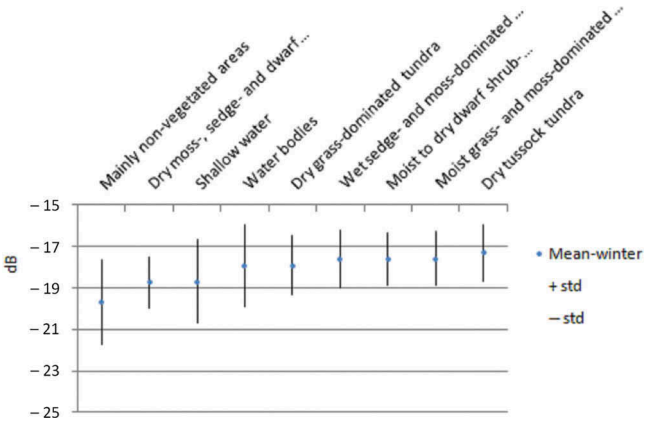

Figure 6. Mean values and standard deviations of $\sigma_{0,\ wmin}$ for the classes of the land-cover map of the Lena Delta by Schneider, Grosse, and Wagner (2009) (for complete class names see Figure 5).

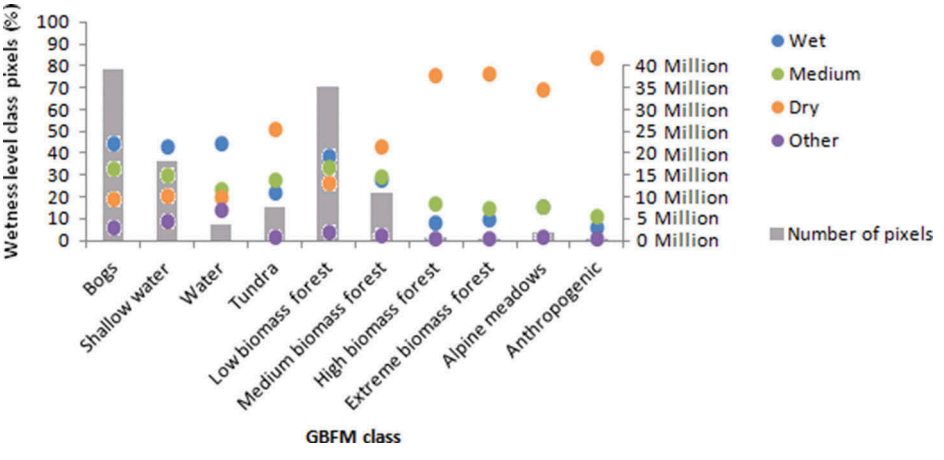

Figure 7. Percentage of wetness level class pixels within GBFM Siberia classes.

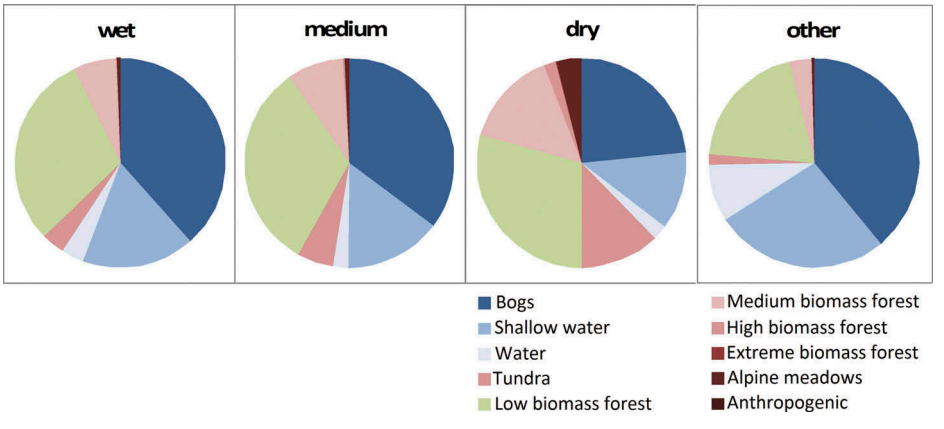

Figure 8. Percentage of GBFM Siberia class pixels within wetness level classes.

3.2.2. GBFM Alaska

For the GBFM Alaskan wetland map not all wetland classes were dominated by wet WL pixels, but those covering the largest areas were still mostly classified correctly (Figure 9). Therefore the wet WL map layer also consisted of more than its half of wetland classes, while in the dry WL class the class 'uplands' was predominant (Figure 10).

3.2.3. USGS Alaska

The USGS Alaskan vegetation map mostly corresponds to the WL map (Figures 11 and 12). Taking the classes 'wet sedge tundra' and 'moist herbaceous/shrub tundra' as wet and the class 'tussock sedge/dwarf shrub tundra' as medium, the WL classes are dominated by their respective vegetation classes. Furthermore, wet vegetation classes show the highest fractions of wet WL pixels. The fact that the water class shows higher fractions of dry WL

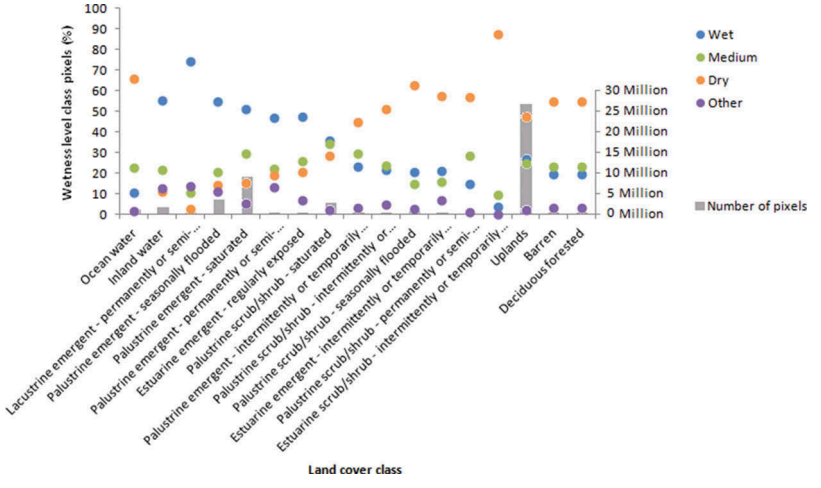

Figure 9. Percentage of wetness level class pixels within GBFM Alaska classes (for complete class names see Figure 10).

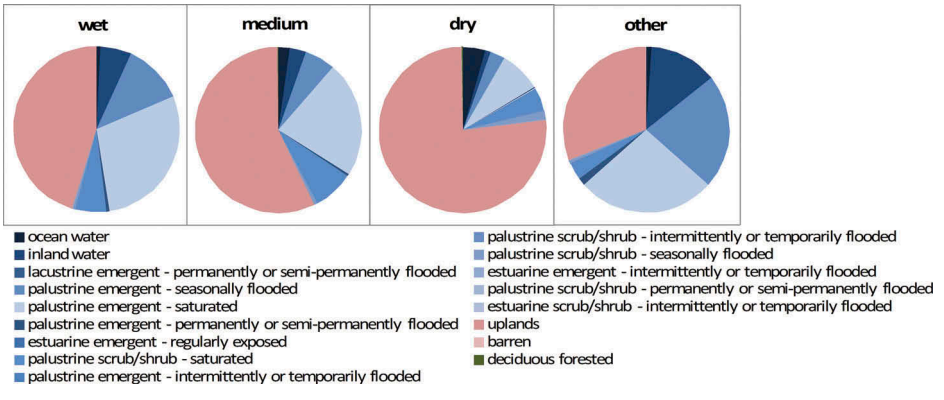

Figure 10. Percentage of GBFM Alaska class pixels within wetness level classes.

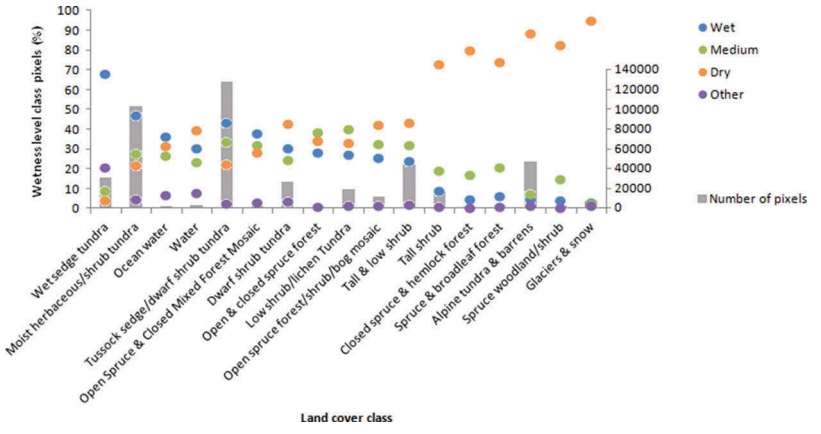

Figure 11. Percentage of wetness level class pixels within the (USGS) vegetation map of Alaska classes.

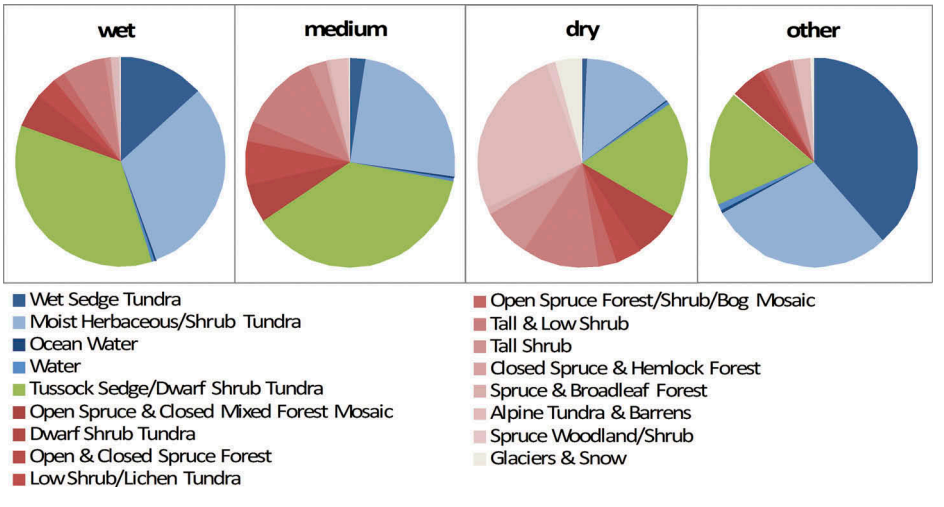

Figure 12. Percentage of (USGS) vegetation map of Alaska class pixels within wetness level classes.

pixels is expected, underlining that water can exhibit somewhat variable backscatter values depending on its freezing status, and should eventually be masked out.

3.2.4. NLCC

For the NLCC map only the classes ‘wet sedge’ and ‘tussock graminoid tundra’ featured a higher content of wet WL pixels, while the class ‘wetland’ was dominated by dry WL pixels (Figure 13). Nevertheless, the wet WL class still showed more definite wet NLCC classes than the dry WL layer (Figure 14).

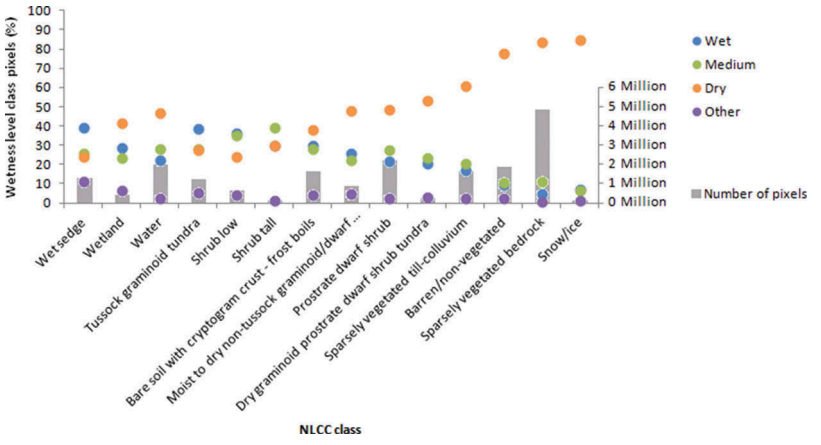

Figure 13. Percentage of wetness level class pixels within the NLCC classes.

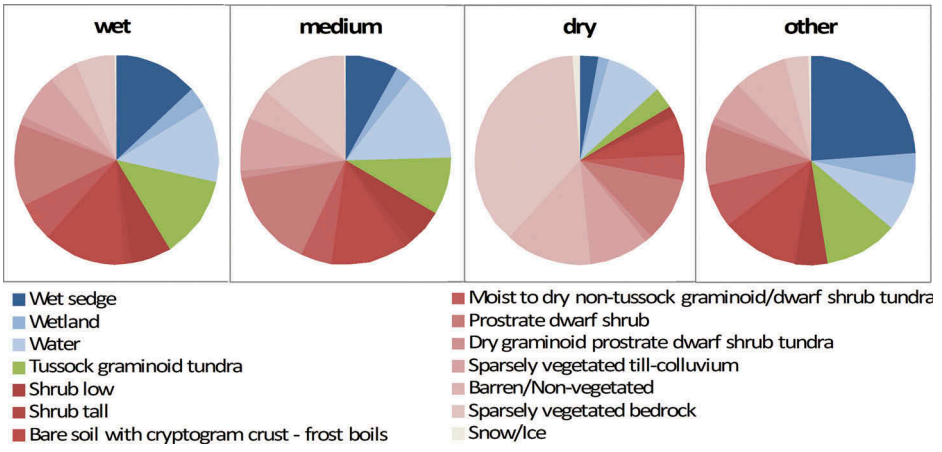

Figure 14. Percentage of NLCC class pixels within wetness level classes.

3.2.5. *Comparison with global maps*

Table 2 shows a comparison of wetland extents derived from the WL map, GLWD, and the CCI land cover map. The wetland area was extracted as a percentage of the total area above the treeline and above 60° N. All maps were divided into western and eastern parts at 10° W, since the GLWD is based on a variety of existing maps, data, and information, and therefore show considerable dependency on their sources. The thematic detail shows specific discrepancies between Russia and North America (Lehner and Döll 2004). In North America three classes of fractional wetlands are available: '50–100% wetland', '25–50% wetland', and 'wetland complex (0–25% wetland)'. For the calculation of the wetland area of these classes the values used were, however, not reduced according to their fractional coverage, but set to 100%. This led to a wetland proportion of 7% for the western part of the GLWD, greatly exceeding the value found for the CCI land-cover product, which only accounts for

Table 2. Comparison of wetland fraction of various sources (GLWD (Lehner and Döll 2004), CCI (ESA (European Space Agency) 2009), Wetness Level map) divided into eastern and western parts at 10° W.

		% wetland of total area (above 60°N and above treeline) [%]	
Source	Classes	West	East
GLWD	• Freshwater marsh • Coastal wetland • Bog, fen, mire • Intermittent wetland • 50–100% wetland • 25–50% wetland	7	5
CCI	• Shrub or herbaceous cover, flooded, fresh/saline/brackish water	1	3
WL map	• Wet	11	30
	• Wet • Medium	21	54

1% wetlands; however, the area covered by the 'wet' WL class identifies 11% of the total area as wetlands. If the 'medium' WL class is also included, 21% is obtained.

For the eastern part, the wetland coverage of the GLWD is again higher than that of the CCI land cover (5 vs. 3%), but not nearly as high as the coverage of the 'wet' WL class. It identifies 30% of the total area as wetland and, by including the WL class 'medium', a percentage of 54 is obtained.

4. Discussion

Although backscatter values increase with soil moisture, the above results show that soil moisture in areas expected to be permanently wet does not have a crucial influence on backscatter values in Arctic regions. As in winter, summer values decrease for wetter areas. As winter values can be comparable to dry summer conditions, it can be assumed that the main influence lies within the roughness and volume scattering within the vegetation, which seems to decrease for land-cover types found in wetter regions. By investigating the difference between summer and winter minimum backscatter $\sigma_{0,\ \mathrm{diff}}$, it can be shown that wet regions show higher values resulting from a greater difference in dielectric constants.

However, the derivation of WLs was shown to be more feasible using the $\sigma_{0,\ \mathrm{wmin}}$ values than $\sigma_{0,\ \mathrm{diff}}$. Due to an overlap of $\sigma_{0,\ \mathrm{diff}}$ values of the wet and medium CAVM classes, their separation within a $\sigma_{0,\ \mathrm{diff}}$-delineated WL map could not be provided.

The reason why the application of $\sigma_{0,\ \mathrm{diff}}$ values for moisture level retrieval was not particularly successful may be due to the fact that wetland-dominated pixels mostly did not show the expected higher values in summer resulting from permanently high soil moisture content. In fact they often exhibited lower winter-like values than other areas, similar to winter conditions. Similar findings were also reported for the L-band-derived Siberian GBFM mosaic. Kropacek and De Grandi (2006) attributed this to the low biomass present in wetlands and specular reflection on the wet soil underneath, which

behaves like a smooth surface. Although the roughness of a surface is dependent on the wavelength used, these findings for the L-band mosaic may also apply to C-band data. Furthermore, it can be expected that less than the entire resolution cell (1 km) is characterized by permanently saturated conditions. Small lakes are characteristic of tundra wetlands and reduce the backscatter (Bartsch et al. 2008; Muster et al. 2013). In addition, C-band backscatter only represents the upper few centimetres and thus represents the fast-drying organic layer on top of the soil.

To date no comparable data set exists that can be used for validation of a WL product. It was nevertheless assessed with circumpolar and regional land-cover maps which identify some classes which can be expected to show wet or moist conditions. These comparisons showed that most wet land-cover classes exhibited higher fractions of wet WL pixels. The class 'medium' may be defined and labelled differently in different products. For instance, in methane flux studies Parmentier et al. (2011) used a 'mixed' class and for the CAVM the middle soil moisture class was labelled as 'moist'. Because the land-cover maps used did not define WL classes, this presented the problem of identifying land-cover classes of the medium WL class. However, in comparison with the underlying CAVM and assuming that 'tussock' classes found elsewhere also represented medium values, it was found that these vegetation classes often showed similar fractions of wet, medium, and dry WL pixels.

Examination of the fractions of vegetation classes within the WL classes confirmed that $\sigma_{0,\ \mathrm{wmin}}$ can be associated with wetland classes. Though the corresponding classes may not always dominate within the respective WL layer, which may be enhanced due to when maps do not show a certain wetness level, it nevertheless became clear that wet vegetation classes had higher percentages within the wet WL class than in the dry one and vice versa.

The only map that was designated to show wetlands was the GBFM thematic map for Alaska. Here wetland areas predominated in the wet WL class, while in the dry WL class the 'uplands' class, considered as dry, was dominant. Similar results were obtained for the USGS vegetation map of the same area.

The WL class 'other' was introduced in order to address discrepancies found in comparison with the vegetation map of the Lena Delta (Schneider, Grosse, and Wagner 2009). The data set of Muster et al. (2012b) shows that this area of the Lena Delta coincides with very low water fraction values, so that the influence of small water bodies can be excluded. The WL class 'other' represents only a small proportion of the final WL map (4%). It is characterized by very low backscatter, which occurs at very flat surfaces. Sandy soils (e.g. coastal areas) are therefore included in this class. Examples of this class can be found at Bunge Land on the Anzhu Islands in Russia or the northern part of the Russian Ayon Islands, which are characterized by sandy coastal areas. The Dewey Soper Bird Sanctuary on the western Baffin Islands in Canada consists of a large proportion of the WL class 'other'. According to the Annotated Ramsar List of Wetlands of International Importance – CANADA (http://www.ramsar.org/countries/canada?page = 5), it is 'an intertidal zone with a series of raised beaches and a marshy plain of mosses and sedges, dotted with shallow lakes and swamps, drained by many small, slow-flowing streams'. There are numerous comparable small patches of the WL class 'other' on the North Slope (Alaska) and around Kytalik (eastern Siberia), which can be matched to river beds and recently drained lakes.

In this context also, the characteristics of open water areas need to be discussed. In cases where open water fails to be masked out it is expected that the WL map will often show dry values due to high winter backscattering values. While frozen rivers mostly exhibit higher backscatter due to rough surfaces resulting from river ice that has been

deformed, lakes can show high values due to double-bounce reflection off tubular bubbles and the ice–water interface, which has a strong dielectric contrast (e.g. Jeffries, Morris, and Liston 1996). Where the ice is frozen to the ground, low backscatter occurs because of the low dielectric contrast between ice and the underlying sediments, in which the signal is lost. Since only December data were used, the percentage of lakes that freeze to the ground is considered to be minimal and only occurs in shallow lakes (Jeffries, Morris, and Liston 1996; Duguay and Lafleur 2003; Surdu et al. 2014). Other effects that can lead to lower backscatter on ice are a smooth air–ice surface or an insufficient number of tubular bubbles (Jeffries, Morris, and Kozlenko 2005).

Since land-cover heterogeneity plays an important role in Arctic areas, ASAR Wide Swath as well as its follow-on sensor Sentinel-1 data provide the opportunity of improvement regarding its higher resolution (150 m). However, this data set is not as abundant in this area and does not provide the same density in its time series as the GM data set.

5. Conclusions

Despite a current need for a representation of spatial wetness patterns in Arctic regions, there are to date no satisfactory circumpolar products. This study demonstrated an easy way to use C-band SAR data in order to derive a circumpolar wetness classification map. By analysing minimum winter and summer backscatter values of Arctic vegetation, dependencies on the vegetation's wetness regime became apparent, allowing a simple hierarchical classification approach. A comparison with land-cover maps indicated the applicability of the WL map, which in consideration of the new C-band Sentinel 1 mission presents further capabilities.

Disclosure statement

No potential conflict of interest was reported by the authors.

Funding

This work was supported by the Austrian Science Fund under Grant [I 1401] (Joint Russian–Austrian project COLD-Yamal) and the PAGE21 project, grant agreement number [282700], funded by the EC Seventh Framework Programme theme FP7-ENV-2011.

References

Alvarez-Mozos, J., J. Casali, M. Gonzalez-Audicana, and N. E. C. Verhoest. 2005. "Correlation between Ground Measured Soil Moisture and RADARSAT-1 Derived Backscatter Coefficient over an Agricultural Catchment of Navarre (North of Spain)." *Biosystems Engineering* 92 (1): 119–133. doi:10.1016/j.biosystemseng.2005.06.008.

Bartsch, A., T. Kumpula, B. Forbes, and F. Stammler. 2010. "Detection of Snow Surface Thawing and Refreezing in the Eurasian Arctic Using QuikSCAT:Iimplications for Reindeer Herding." *Ecological Applications* 20 (8): 2346–2358. doi:10.1890/09-1927.

Bartsch, A., C. Pathe, W. Wagner, and K. Scipal. 2008. "Detection of Permanent Open Water Surfaces in Central Siberia with ENVISAT ASAR Wide Swath Data with Special Emphasis on the Estimation of Methane Fluxes from Tundra Wetlands." *Hydrology Research* 39 (2): 89–100. doi:10.2166/nh.2008.041.

Bartsch, A., A. M. Trofaier, G. Hayman, D. Sabel, S. Schlaffer, D. Clark, and E. Blyth. 2012. "Detection of Open Water Dynamics with ENVISAT ASAR in Support of Land Surface Modelling at High Latitudes." *Biogeosciences* 9: 703–714. doi:10.5194/bg-9-703-2012.

Bartsch, A., W. Wagner, C. Pathe, K. Scipal, D. Sabel, and P. Wolski. 2009. "Global Monitoring of Wetlands - the Value of ENVISAT ASAR Global Mode." *Journal of Environmental Management* 90 (7): 2226–2233. doi:10.1016/j.jenvman.2007.06.023.

Bicheron, P., P. Defourny, C. Brockmann, L. Schouten, C. Vancutsem, M. Huc, and S. Bontemps, et al. 2008. *GlobCover: Products Description and Validation Report*. Toulouse: MEDIAS-France.

CAVM Team. 2003. *Circumpolar Arctic Vegetation Map. Scale 1:7,500,000.Conservation of Arctic Flora and Fauna (CAFF) Map No. 1*.. Anchorage, AK: U.S. Fish and Wildlife Service.

Duguay, C. R., and P. M. Lafleur. 2003. "Determining Depth and Ice Thickness of Shallow Sub-Arctic Lakes using Space-borne Optical and SAR Data." *International Journal of Remote Sensing* 24 (3): 475–489. doi:10.1080/01431160304992.

Duguay, C. R., T. Zhang, D. W. Leverington, and V. E. Romanovsky. 2005. "Satellite Remote Sensing of Permafrost and Seasonally Frozen Ground." In *Remote Sensing in Northern Hydrology: Measuring Environmental Change*, edited by C. R. Duguay, and A. Pietroniro. Washington, DC: American Geophysical Union.

Durden, S. L., Z. S. Haddad, L. A. Morrissey, and G. P. Livingston. 1996. "Classification of Radar Imagery over Boreal Regions for Methane Exchange Studies." *International Journal of Remote Sensing* 17 (6): 1267–1273. doi:10.1080/01431169608949086.

Engman, E. T. 2000. "Soil Moisture." In *Remote Sensing in Hydrology and Water Management*, edited by G. A. Schultz, and E. T. Engman, 197–216. Berlin: Springer.

ESA (European Space Agency). 2004. *ENVISAT ASAR Product Handbook*. ESA.

ESA (European Space Agency). 2009. ESA Climate Change Initiative Description, EOP-SEP/TN/0030-09/SP, Technical Note. September 30, 2009.

Henderson, F. M., and A. J. Lewis, eds. 1998. *Principles and Applications of Imaging Radar*. Vol. 2 *of Manual of Remote Sensing*. 3rd ed. New York: Wiley. American Society for Photogrammetry and Remote Sensing.

Högström, E., A. M. Trofaier, I. Gouttevin, and A. Bartsch. 2014. "Assessing Seasonal Backscatter Variations with Respect to Uncertainties in Soil Moisture Retrieval in Siberian Tundra Regions." *Remote Sensing* 6 (9): 8718–8738. doi:10.3390/rs6098718.

Jeffries, M. O., K. Morris, and N. Kozlenko. 2005. "Ice Characteristics and Processes, and Remote Sensing of Frozen Rivers and Lakes." In *Remote Sensing in Northern Hydrology: Measuring Environmental Change*, edited by C. R. Duguay, and A. Pietroniro. Washington, DC: American Geophysical Union.

Jeffries, M. O., K. Morris, and G. E. Liston. 1996. "A Method to Determine Lake Depth and Water Availability on the North Slope of Alaska with Spaceborne Imaging Radar and Numerical Ice Growth Modelling." *Arctic* 49 (4): 367–374. doi:10.14430/arctic1212.

Jones, B. M., G. Grosse, C. D. Arp, M. C. Jones, K. M. Walter Anthony, and V. E. Romanovsky. 2011. "Modern Thermokarst Lake Dynamics in the Continuous Permafrost Zone, Northern Seward Peninsula, Alaska." *Journal of Geophysical Research* 116 (G2). doi:10.1029/2011JG001666.

Kerr, Y. H., P. Waldteufel, J.-P. Wigneron, J. Martinuzzi, J. Font, and M. Berger. 2001. "Soil Moisture Retrieval from Space: The Soil Moisture and Ocean Salinity (SMOS) Mission." *IEEE Transactions on Geoscience and Remote Sensing* 39 (8): 1729–1735. doi:10.1109/36.942551.

Koven, C. D., B. Ringeval, P. Friedlingstein, P. Ciais, P. Cadule, D. Khvorostyanov, G. Krinner, and C. Tarnocai. 2011. "Permafrost Carbon-Climate Feedbacks Accelerate Global Warming." *Proceedings of the National Academy of Sciences* 108 (36): 14769–14774. doi:10.1073/pnas.1103910108.

Krankina, O. N., D. Pflugmacher, D. J. Hayes, A. D. McGuire, M. C. Hansen, T. Häme, V. Elsakov, and P. Nelson. 2011. "Vegetation Cover in the Eurasian Arctic: Distribution, Monitoring, and Role in Carbon Cycling." In *Eurasian Arctic Land Cover and Land Use in a Changing Climate* edited by G. Gutman and A. Reissell, 79–108. New York: Springer.

Kropacek, J., and G. De Grandi. 2006. "Wetlands Mapping in Siberia by Classification of the GBFM Radar Mosaic Using Backscatter and Terrain Topographic Features." In *Proceedings of the Conference GlobWetland: Looking at Wetlands from Space* edited by H. Lacoste. Frascati: ESA Publications Division.

Lehner, B., and P. Döll. 2004. "Development and Validation of a Global Database of Lakes, Reservoirs and Wetlands." *Journal of Hydrology* 296 (1–4): 1–22. doi:10.1016/j.jhydrol.2004.03.028.

Moran, M. S., D. C. Hymer, J. Qi, and E. E. Sano. 2000. "Soil Moisture Evaluation Using Multi-Temporal Synthetic Aperture Radar (SAR) in Semiarid Rangeland." *Agricultural and Forest Meteorology* 105 (1–3): 69–80. doi:10.1016/S0168-1923(00)00189-1.

Morrissey, L. A., S. L. Durden, G. P. Livingston, J. A. Steam, and L. S. Guild. 1996. "Differentiating Methane Source Areas in Arctic Environments with Multitemporal ERS-1 SAR Data." *IEEE Transactions on Geoscience and Remote Sensing* 34 (3): 667–673. doi:10.1109/36.499746.

Muster, S., B. Heim, A. Abnizova, and J. Boike. 2013. "Water Body Distributions Across Scales: A Remote Sensing Based Comparison of Three Arctic Tundra Wetlands." *Remote Sensing* 5 (4): 1498–1523. doi:10.3390/rs5041498.

Muster, S., M. Langer, B. Heim, S. Westermann, and J. Boike. 2012a. "Landsat Subpixel Water Cover of Lena River Delta, Siberia, with Link to ESRI Grid Files." doi:10.1594/PANGAEA.786926. In Supplement to: "Subpixel Heterogeneity of Ice-Wedge Polygonal Tundra: A Multi-Scale Analysis of Land Cover and Evapotranspiration in the Lena River Delta, Siberia." *Tellus Series B-Chemical and Physical Meteorology* 64 (17301). doi:10.3402/tellusb.v64i0.17301.

Muster, S., M. Langer, B. Heim, S. Westermann, and J. Boike. 2012b. "Subpixel Heterogeneity of Ice-Wedge Polygonal Tundra: A Multi-Scale Analysis of Land Cover and Evapotranspiration in the Lena River Delta, Siberia." *Tellus Series B-Chemical and Physical Meteorology* 64 (17301). doi:10.3402/tellusb.v64i0.17301.

Naeimi, V., Z. Bartalis, and W. Wagner. 2009a. "ASCAT Soil Moisture: An Assessment of the Data Quality and Consistency with the ERS Scatterometer Heritage." *Journal Of Hydrometeorology* 10 (2): 555–563. doi:10.1175/2008JHM1051.1.

Naeimi, V., C. Paulik, A. Bartsch, W. Wagner, R. Kidd, S. Park, K. Elger, and J. Boike. 2012. "ASCAT Surface State Flag (SSF): Extracting Information on Surface Freeze/Thaw Conditions from Backscatter Data Using an Empirical Threshold-Analysis Algorithm." *IEEE Transactions on Geoscience and Remote Sensing* 50 (7): 2566–2582. doi:10.1109/TGRS.2011.2177667.

Naeimi, V., K. Scipal, Z. Bartalis, S. Hasenauer, and W. Wagner. 2009b. "An Improved Soil Moisture Retrieval Algorithm for ERS and METOP Scatterometer Observations." *IEEE Transactions on Geoscience and Remote Sensing* 47 (7): 1999–2013. doi:10.1109/TGRS.2008.2011617.

Njoku, E. G. 2004. *AMSR-E/Aqua Daily L3 Surface Soil Moisture, Interpretive Parameters, & QC EASE-Grids*. Version 2.Boulder, CO: NASA DAAC at the National Snow and Ice Data Center.

Olthof, I., R. Latifovic, and D. Pouliot. 2009. "Development of a Circa 2000 Land Cover Map of Northern Canada at 30 m Resolution from Landsat." *Canadian Journal of Remote Sensing: Journal Canadien De Télédétection* 35 (2): 152–165. doi:10.5589/m09-007.

Park, S.-E., A. Bartsch, D. Sabel, W. Wagner, V. Naeimi, and Y. Yamaguchi. 2011. "Monitoring Freeze/Thaw Cycles Using ENVISAT ASAR Global Mode." *Remote Sensing of Environment* 115 (12): 3457–3467. doi:10.1016/j.rse.2011.08.009.

Parmentier, F. J. W., J. van Huissteden, M. K. van der Molen, G. Schaepman-Strub, S. A. Karsanaev, T. C. Maximov, and A. J. Dolman. 2011. "Spatial and Temporal Dynamics in Eddy Covariance Observations of Methane Fluxes at a Tundra Site in Northeastern Siberia." *Journal of Geophysical Research* 116 (G3). doi:10.1029/2010JG001637.

Pathe, C., W. Wagner, D. Sabel, M. Doubkova, and J. Basara. 2009. "Using ENVISAT ASAR Global Mode Data for Surface Soil Moisture Retrieval over Oklahoma, USA." *IEEE Transactions on Geoscience and Remote Sensing* 47 (2): 468–480. doi:10.1109/TGRS.2008.2004711.

Pflugmacher, D., O. N. Krankina, W. B. Cohen, M. A. Friedl, D. Sulla-Menashe, R. E. Kennedy, and P. Nelson, et al. 2011. "Comparison and Assessment of Coarse Resolution Land Cover Maps for Northern Eurasia." *Remote Sensing of Environment* 115 (12): 3539–3553. doi:10.1016/j.rse.2011.08.016.

Prigent, C., F. Papa, F. Aires, W. B. Rossow, and E. Matthews. 2007. "Global Inundation Dynamics Inferred from Multiple Satellite Observations, 1993–2000." *Journal of Geophysical Research* 112: D12. doi:10.1029/2006JD007847.

Reschke, J., A. Bartsch, S. Schlaffer, and D. Schepaschenko. 2012. "Capability of C-Band SAR for Operational Wetland Monitoring at High Latitudes." *Remote Sensing* 4 (10): 2923–2943. doi:10.3390/rs4102923.

Ringeval, B., N. de Noblet-Ducoudre, P. Ciais, P. Bousquet, C. Prigent, F. Papa, and W. B. Rossow. 2010. "An Attempt to Quantify the Impact of Changes in Wetland Extent on Methane Emissions on the Seasonal and Interannual Time Scales." *Global Biogeochemical Cycles* 24 (2). doi:10.1029/2008GB003354.

Sabel, D., Z. Bartalis, W. Wagner, M. Doubkova, and J. P. Klein. 2012. "Development of a Global Backscatter Model in Support to the Sentinel - 1 Mission Design." *Remote Sensing of Environment* 120: 102–112. doi:10.1016/j.rse.2011.09.028.

Sabel, D., C. Pathe, W. Wagner, S. Hasenauer, A. Bartsch, C. Künzer, and K. Scipal. 2007. "Using ENVISAT ScanSAR Data for Characterizing Scaling Properties of Scatterometer Derived Soil Moisture Information over Southern Africa." In *Proceedings of the Envisat Symposium*, edited by H. Lacoste and L. Owehand. Montreux: ESA. ESA SP - 636.

Schneider, J., G. Grosse, and D. Wagner. 2009. "The Lena River Delta - Land Cover Classification of Tundra Environments Based on Landsat 7 ETM+ Data and Its Application for Upscaling of Methane Emissions." doi:10.1594/PANGAEA.759631. In Supplement to: "Land Cover Classification of Tundra Environments in the Arctic Lena Delta Based on Landsat 7 ETM+ Data and its Application for Upscaling of Methane Emissions." *Remote Sensing of Environment* 113 (2): 380–391. doi:10.1016/j.rse.2008.10.013.

Schroeder, R., M. A. Rawlins, K. C. McDonald, E. Podest, R. Zimmermann, and M. Kueppers. 2010. "Satellite Microwave Remote Sensing of North Eurasian Inundation Dynamics: Development of Coarse-Resolution Products and Comparison with High-Resolution Synthetic Aperture Radar Data." *Environmental Research Letters* 5: 1. doi:10.1088/1748-9326/5/1/015003.

Surdu, C. M., C. R. Duguay, L. C. BrownFernández, and D. Prieto. 2014. "Response of Ice Cover on Shallow Lakes of the North Slope of Alaska to Contemporary Climate Conditions (1950–2011): Radar Remote-Sensing and Numerical Modeling Data Analysis." *The Cryosphere* 8: 167–180. doi:10.5194/tc-8-167-2014.

Ulaby, F. T., R. K. Moore, and A. K. Fung. 1982. *Radar Remote Sensing and Surface Scattering and Emission Theory* Vol. 2 *of Microwave Remote Sensing: Active and Passive*. Norwood, MA: Artech House.

van Huissteden, J., and A. J. Dolman. 2012. "Soil Carbon in the Arctic and the Permafrost Carbon Feedback." *Current Opinion in Environmental Sustainability* 4 (5): 545–551. doi:10.1016/j.cosust.2012.09.008.

Wagner, W., G. Lemoine, and H. Rott. 1999. "A Method for Estimating Soil Moisture from ERS Scatterometer and Soil Data." *Remote Sensing of Environment* 70 (2): 191–207. doi:10.1016/S0034-4257(99)00036-X.

Walker, D. A., W. A. Gould, H. A. Maier, and M. K. Raynolds. 2002. "The Circumpolar Arctic Vegetation Map: AVHRR-Derived Base Maps, Environmental Controls, and Integrated Mapping Procedures." *International Journal of Remote Sensing* 23 (21): 4551–4570. doi:10.1080/01431160110113854.

Watts, J. D., J. S. Kimball, A. Bartsch, and K. C. McDonald. 2014. "Surface Water Inundation in the Boreal-Arctic: Potential Impacts on Regional Methane Emissions." *Environmental Research Letters* 9 (7): 075001. doi:10.1088/1748-9326/9/7/075001.

Whitcomb, J., M. Moghaddam, K. McDonald, J. Kellndorfer, and E. Podest. 2009. "Mapping Vegetated Wetlands of Alaska Using L-Band Radar Satellite Imagery." *Canadian Journal of Remote Sensing: Journal Canadien De Télédétection* 35 (1): 54–72. doi:10.5589/m08-080.